Aging and Temperature Effects on the Performance of Sustainable One-Part Geopolymers Developed for Well-Cementing Applications

Mohamed Omran[1]*, Mahmoud Khalifeh[1], and Maria Paiva[2]

[1]Department of Energy and Petroleum Eng, Faculty of Science and Technology, University of Stavanger
[2]Sustainable Materials Research Center (NUMATS), Federal University of Rio de Janeiro

Summary

This study elucidates the effects of aging and temperature over the performance of one-part "just add water" (JAW) granite-based geopolymers for application in well cementing and well abandonment. Additionally, the investigation delves into the fluid-state and early-age solid-state properties of these geopolymers, with a particular emphasis on their performance after aging. The aging process extended up to 56 days for assessing mechanical properties and up to 28 days for evaluating hydraulic sealability through dedicated tests. The obtained results unveil a nonlinear correlation between the designated temperature and pumping duration. Notably, the issue of fluid loss emerged as a significant concern for these geopolymers. The early-age strength development of the mix design containing zinc demonstrates adherence to industry norms by achieving minimal strength requirements within 24 hours of curing. Zinc plays a pivotal role as a strength enhancer during the initial curing stages of geopolymers, both under ambient conditions and at elevated temperatures (70°C). However, upon extended curing at elevated temperatures, zinc's impact slightly diminishes compared with the unmodified mix design. After around 30 days of curing, a consecutive reaction occurs in both the unmodified and zinc-modified mix designs. Aging leads to a decline in the material's hydraulic sealability that was initially established during the early stages of curing.

Introduction

In recent years, there has been a rapid increase in the demand for cement production. A 2016 report estimated that the emission of greenhouse gases from the cement industry alone could be responsible for up to 8% of global carbon dioxide emissions (Gilfillan and Marland 2021). Despite efforts to improve efficiency and promote cleaner cement production, the energy-intensive process of cement clinker calcination remains a necessity (Mo et al. 2010). Therefore, the development of sustainable and viable alternative materials that can fully replace ordinary Portland cement (OPC) while possessing equal or superior chemophysical properties remains the most effective strategy (Luukkonen et al. 2018; Omran and Khalifeh 2023).

Alkali-activated materials (AAM) and geopolymers have been recognized as environmentally friendly alternatives to replace OPC. It is believed that their production results in 50–70% lower carbon dioxide emissions per ton of the produced material when compared with that of OPC (McLellan et al. 2011; Mellado et al. 2014). Moreover, the production of these materials aligns with the principles of circular economy when byproducts are utilized as precursors. Extensive research has been conducted on various types of geopolymers. Depending on the specific type and mix design, geopolymers exhibit improved resistance to acids and sulfates, enhanced heat resistance, reduced chemical shrinkage, and stronger mechanical properties when compared with OPC (Luukkonen et al. 2018).

Conventional geopolymers are typically produced using a "two-part" mixture, consisting of an alkaline or alkali silicate solution and a solid precursor that contains amorphous aluminosilicates. While the two-part geopolymer exhibits excellent properties compared with OPC (Chamssine 2023; Gomado et al. 2023; Khalifeh 2016; Khalifeh et al. 2018, 2019; Paiva et al. 2018; Salehi et al. 2018), its application is limited to precast operations due to logistical and health, safety, and environmental constraints arising from the high pH of the activator solution. In other words, the drawback of the two-part geopolymer system is the requirement for a user-hostile and highly corrosive activator solution, which poses potential risks and restricts its use in mass production and large-scale applications, particularly in the oil and gas industry (Luukkonen et al. 2018; Nematollahi et al. 2015).

"One-part" geopolymers, also known as "JAW" geopolymers, can be seen as the evolution of two-part geopolymers, effectively addressing the limitations caused by the high pH liquid activator. Unlike two-part geopolymers, JAW geopolymers only require the addition of water along with the dry ingredients (Luukkonen et al. 2018; Nematollahi et al. 2015; Omran and Khalifeh 2023; Singh and Middendorf 2020). This concept was initially introduced by Hajimohammadi et al. (2008). Afterward, extensive research and development have been carried out by various researchers on one-part geopolymers, leading to the proposal of different geopolymer mix designs. These investigations have focused on the geopolymer cement synthesis using industrial and natural aluminosilicate sources, mainly composed of fly ash slag and metakaolin, that are normalized when needed with complementary Si and Al reactive sources, such as synthetic and agroindustrial ashes. More recently, various Al- and Si-rich residues, such as mine tailings, bauxite, rock backfill, demolition waste, sewage, and sludge materials, have also been adopted as geopolymer precursors (Nematollahi et al. 2015; Singh and Middendorf 2020).

Several factors, including curing temperature and aging, directly affect geopolymers through the geopolymerization process and its performance (Adam and Horianto 2014; Cai et al. 2020; Chithiraputhiran and Neithalath 2013; Hajimohammadi et al. 2011; Hajimohammadi and van Deventer 2017; Ke et al. 2015; Kong and Sanjayan 2010; Li et al. 2013; Luukkonen et al. 2018; Omran et al.

*Corresponding author; email: mohamed.a.omran@uis.no

Original SPE manuscript received for review 6 August 2023. Revised manuscript received for review 11 September 2023. Paper (SPE 217993) peer approved 26 September 2023.

2023aOmran et al. 2023b; Pilehvar et al. 2020; Rovnaník 2010; Sun and Vollpracht 2019). **Table 1** presents a compilation of relevant literature from previous research endeavors, providing a summary of their significant findings in the respective field of study.

Title	Geopolymer System	Significant Outputs
One-part geopolymer mixes from geothermal silica and sodium aluminate (Hajimohammadi et al. 2008)	One-part	● Purified and milled geothermal silica was utilized as an Si-rich precursor and then activated by various concentrations of solid sodium aluminate and water/solid ratios. ● Lower water content in the system increased the degree of crystallinity with 2 weeks of aging at 40°C. ● The high aluminum content can hinder the geopolymerization reaction by causing the sorption of aluminum onto the silica surface, thereby impeding its dissolution.
One-part geopolymers based on thermally treated red mud/NaOH blends (Ke et al. 2015)	One-part	● An alkali-thermal activation process was investigated for an aluminum- and calcium-rich red mud base JAW system. ● Sodium hydroxide in pellet form was calcined with red mud at 800°CC, leading to the formation of calcium-rich phases, such as C_3A, and α-C_2S. Additionally, this process promoted the formation of a partially peralkaline Na-aluminosilicate phase. ● Na-rich aluminosilicate salts can supply an adequate number of alkalis during the dissolution process, thereby enhancing the reactivity. ● The excess of alkalis in the system resulted in limited strength development and efflorescence, which were identified as shortcomings.
Characterisation of one-part geopolymer binders made from fly ash (Hajimohammadi and van Deventer 2017)	One-part	● A low calcium content fly ash was activated by various concentrations of solid sodium silicates and sodium hydroxide and different water contents. ● The reaction mechanisms and physical properties of the system were investigated after curing the samples at 40°C for up to 3 weeks. ● The higher the Si/Al ratio of the binder design, the denser the geopolymer microstructure. ● A lower water content leads to increased participation of Si in the final geopolymer gel, thereby achieving optimal mechanical performance.
Time-resolved and spatially resolved infrared spectroscopic observation of seeded nucleation controlling geopolymer gel formation (Hajimohammadi et al. 2011)	One-part	● A milled geothermal silica precursor and a solid sodium aluminate activator were seeded with various types of oxide nanoparticles, the samples were cured at 40°C for up to 3 weeks. ● The addition of ZnO nanoparticles enhances the mechanical properties of the JAW mix design, particularly during the early age performance, when compared with the unseeded mix design. ● The seeding process enhances the dissolution of silica and enables control over silica release rates in the initially aluminum-rich reaction mixture, thereby allowing engineering structure and physical properties of the geopolymers. ● The seeding process enhances the geopolymer nucleation stage by hindering the sorption of aluminum on the silica surface.
Synthesis of sustainable one-part geopolymers for well cementing applications (Omran et al. 2023a)	One-part	● Presents a synthesis of granite-based geopolymers normalized with slag in different ratios. ● The use of slag increases the viscosity and consistency of the slurry, it has an optimum working range of up to 47 wt%. ● Exceeding the optimal slag content, overexpansion and detrimental physical properties are expected. ● Considering the early age properties of the geopolymers, granite mainly works as a filler.
Design and early age performance of sustainable one-part geopolymers for well cementing (Omran et al. 2023b)	One-part	● ZnO acts as an early strength booster by increasing the rate of heat evolution, thereby satisfying the early age properties required for cementing wells. ● The dissolution rate of the solid activator is a parameter that needs to be considered. ● By combining the solid activator and granite, Si and Al are released, which is an indication of granite dissolution.
One-part alkali-activated materials for construction – a review (Mahendra and Narasimhan 2023)	One-part	● The primary components of one-part geopolymers often consist of precursors such as fly ash and ground granulated blast furnace slag. ● The reaction can lead to the precipitation of various gel forms, including C/Na-A-S-H. ● In comparison with two-part systems, the release rates of Si and Al species are generally slower in one-part systems. ● Introducing water gradually has shown to be more efficacious than adding all the water at once.

Table 1—Examples of published literature reviews and articles on the different effects of temperature, curing conditions, and curing duration on alkali-activated geopolymer cement.

To develop a commercially viable and sustainable geopolymer, one should consider the technoeconomical aspects of the precursors to be used. One of the main drivers to make the geopolymers more attractive nowadays is to reduce the greenhouse gas emissions from their synthesis, the availability and transportation of the raw materials, and also their precursors' beneficiation, as well as their activators' preparation impacts. In an effort, Khalifeh (2016) and Khalifeh et al. (2018, 2019) first developed two-part granite-based geopolymers to replace OPC used in well construction and well abandonment operations.

As the health, safety, and environmental limitations of the two-part system were identified, Omran and Khalifeh (Omran and Khalifeh 2022) developed a one-part granite-based geopolymer. performed further studies, in the fluid-state and early age solid-state properties of the one-part granite-based geopolymers, revealing the potential of the developed technology for in-situ applications with adjustable properties. Experimental studies show that the use of sodium salts of naphthalene-sulfonic acid-containing formaldehyde dispersants and sodium lignosulfonates are effective superplasticizers for this type of geopolymer (Hjelm 2022; Omran et al. 2022b).

The above-mentioned articles, along with the limited number of accessible papers on one-part geopolymers, highlight the need for further research on the topic of one-part geopolymers. Additionally, there is a lack of research on the impact of elevated temperature and long aging on the final properties of the developed geopolymers.

This work aims to investigate the effect of temperature and long curing time on the properties and performance of the one-part granite-based geopolymers to better understand the mechanism of zinc in the one-part geopolymer design.

Materials and Methods

Materials. The neat JAW geopolymer is based on both solid precursors and solid activator components, which together are mixed with distilled water to create the cementitious geopolymer system. The materials in the precursor were ground granite rock; a ground granulated blast furnace slag (GGBFS) rich in aluminum, calcium, and magnesium; and microsilica (MS), which is an almost pure amorphous silica source. The dissolution rate and their role in the mix design has been published in previous works (Omran et al. 2023a, 2023b; Omran and Khalifeh 2023).

The chemical composition of the raw materials and the neat JAW precursor has been tabulated in **Table 2**. The activator was prepared using anhydrous potassium silicate and potassium hydroxide in powder form with a final molar ratio (SiO_2/K_2O) of 2.4. In addition to analyzing the neat JAW recipe, zinc oxide was introduced together with the precursor as an additive for improving the mechanical properties of the geopolymer cement. The physical properties of the precursor and other mixture components are presented in **Table 3**.

Chemical Composition (wt%)*	Granite	GGBFS	MS	JAW Precursor Mixture
SiO_2	73.44	35.78	95.50	56.63
Al_2O_3	13.33	12.72	0.70	12.47
Fe_2O_3	2.06	0.18	0.30	1.09
MgO	0.44	12.77	0.50	6.23
CaO	1.12	33.74	0.40	16.45
Na_2O	3.12	0.55	0.40	1.77
K_2O	5.11	0.82	1.00	2.87
TiO_2	0.23	2.23	0.00	1.16
MnO	0.04	0.58	0.00	0.29
LOI†	0.90	0.30	2.00	0.60

*By weight of the total precursor mixture.
†Loss of ignition.

Table 2—Chemical composition of the JAW geopolymer precursor (Omran et al. 2023b).

Physical Properties	d10 (μm)	d50 (μm)	d90 (μm)	Specific Gravity (g/cm^3)	Specific Surface Area (m^2/kg)
Granite	3.52	21.1	131	2.63	631
GGBFS	2.79	15.9	46.6	2.90	944
MS	0.19	0.34	0.60	2.29	19 320
K_2SiO_3	5.16	33.3	101	2.37	487
ZnO	0.55	2.06	106	5.61	3810

d10, d50, d90, particle-size distribution percentiles.

Table 3—Physical properties of all components in the geopolymer system.

Mix Design. In this work, two previously developed recipes "JAW" and "JAW-Z" have been studied (Omran et al. 2023a, 2023b) and listed in **Tables 4 and 5**. JAW-Z was selected among other zinc oxide (ZnO) concentrations evaluated previously because it showed the best early age performance.

Composition (% bwop*)	JAW	JAW-Z (JAW + 0.86% ZnO)
Granite	48.6	48.6
GGBFS	47.1	47.1
MS	4.29	4.29
K_2SiO_3	20.8	20.8
KOH (anhydrous)	4.24	4.24
ZnO	0.00	0.86
Water	41.3	41.3
Source	Omran et al. 2023b	Omran et al. 2023b

*By weight of precursor mixture (granite, GGBFS, and MS).

Table 4—Geopolymer formulations investigated in this study.

Molar ratios	JAW	JAW-Z
$SiO_{2,nominal}$ /Al_2O_3	9.72	9.72
$SiO_{2,reactive}$ /Al_2O_3	4.87	4.87
$SiO_{2,nominal}$ /CaO	4.05	4.05
$SiO_{2,reactive}$ /CaO	2.03	2.03
K_2O/Al_2O_3	1.07	1.07
Na_2O/Al_2O_3	0.23	0.23
$(K_2O + Na_2O)/Al_2O_3$	1.31	1.31
$ZnO/SiO_{2,nominal}$	–	0.0088
$ZnO/SiO_{2,reactive}$	–	0.0175
ZnO/CaO	–	0.0355
H_2O/K_2O	17.75	17.78
Water/solid	0.33	0.33
Specific gravity (g/cm^3)	1.88	1.89

Table 5—Oxide molar ratios, water/solid ratios, and theoretical density of geopolymer formulations.

Methods. Mixing procedure, thickening time, differential scanning calorimetry (DSC), ultrasonic compressive strength (UCA), uniaxial compressive strength (UCS), alkalinity and inductively coupled plasma, X-ray diffraction (XRD), and Fourier-transform infrared spectroscopy (FTIR) methodologies are described in detail on previous study (Omran et al. 2023b). A pressurized mud balance was used to estimate slurry density (*API RP 10B-2* 2019). Hydraulic sealability test methodology, on the other hand, can be found in the work done by Gomado et al. (2023).

Viscosity and API Gel-Strength Measurements. The rheological behavior of the slurries was assessed at 25°C by using a viscometer (viscosity-gel, VG) according to the specifications of the American Petroleum Institute (*API RP 10B-2* 2019). studied the rheology of granite-based geopolymers where the Herschel-Bulkley model was applied successfully.

Static Fluid Loss Test. An API fluid loss test (FLT) cell was used to measure the fluid loss at 69 bar (1,000 psi) in ambient temperature (*API RP 10B-2* 2019). A sieve with a mesh grid of 250 μm and a hardened filter was used together. The hardened filter was used to facilitate sampling for further analysis. The test was running for 30 minutes. Afterward, the produced fluids have been collected and examined as pore solution for pH and inductively coupled plasma spectroscopy analysis.

Hydraulic Sealability Test. Due to volume limitations, a Hobart N50-60 commercial mixer was used for hydraulic sealability tests. The precursors were introduced to deionized water at Level 1 stirring speed and then stirred continuously for 25 minutes at Level 2 stirring speed. Then, slurries were poured and cured inside hydraulic sealability test cells at 37.5 bar and 25°C. Once the geopolymer cement had fully cured, nitrogen gas was connected to the bottom of the test cell, which then is connected to the separator, flowmeters, and the data logging system. The plugs within the hydraulic test cell were then pressure tested with increments of 5 bar at a time to test their sealing ability. Details of the test setup and test protocols have been published by Gomado et al. (2023).

Scanning Electron Microscope. To analyze and reveal microstructure of the geopolymers, a scanning electron microscope (SEM) was used at backscattered electrons (BSE) and secondary electrons (SE) modes. SEM analysis was performed on the remains of each crushed geopolymer specimen after performing UCS tests at the final day of aging (7 days–2 months). Before coating, all samples were dried the same way as the samples for XRD. Then, the samples were coated with an 11-nm palladium plasma to prevent the samples from charging during the experiment.

Results and Discussion

Early Age Properties Characterization. ***Slurry Characteristics.*** **Fig. 1** and **Table 6** present the rheological properties of JAW and JAW-Z. Both recipes have very comparable rheological behavior. The slurries are both behaving shear thinning pastes. The measurements do not indicate sign of particle settling. **Table 7** presents a summary of the other slurry properties measured right after mixing, including slurries' pH, density, zeta potential, and initial consistency. These parameters are also comparable for both mixes. Additionally, the pore solution was collected and examined for both mixes and the ones from Omran et al. 2023b) after performing the FLT, which can be seen in **Table 8** and **Fig. 2**.

The static fluid loss for both neat and 0.86% ZnO JAW (as well as the ones from Omran et al. 2023b) reveals higher values than the limits outlined from *API RP 10B-2* (2019) and not observed at all for the two-part granite-based geopolymers (Chamssine 2023). Thus, fluid loss control additives shall be tested in combination with the JAW geopolymers.

The inductively coupled plasma spectrometry analysis, see **Fig. 2**, shows that the zinc contributes to facilitate the dissolution of aluminum species to some extent while simultaneously lowers the availability of silicon species in the pore solution due to the consumption of free silicon ions through the formation of zincates. That was further investigated by Anseau et al. (2005), Chen et al. (2012), Hajimohammadi et al. (2011), and summarized by Omran et al. (2023b). Thus, it favors the geopolymerization process by lowering the Si/Al ratio from 10 to 3.

Conditioning and Thickening Time. **Fig. 3** and **Table 9** show effect of 20, 30, 40, and 50°C bottomhole circulating temperature (BHCT) on the thickening time for the given two recipes and the ones from Omran et al. 2023b). All the examined slurries of the JAW system set and harden rapidly, typically within minutes, once they reach a consistency between 40 and 50 Bc. Therefore, 40 Bc was selected as the pumpability time for all pastes, and the tests were concluded at this point. All JAW recipes exhibited a right-angle set phenomenon within a bottomhole circulating temperature range of 20–50°C.

Both recipes have very comparable initial consistency results at each temperature assessed, as detailed in **Table 9**. Lower BHCT has a clear effect on elongating the pumpability duration for both recipes, i.e., the slurry is temperature-sensitive. This behavior has been also

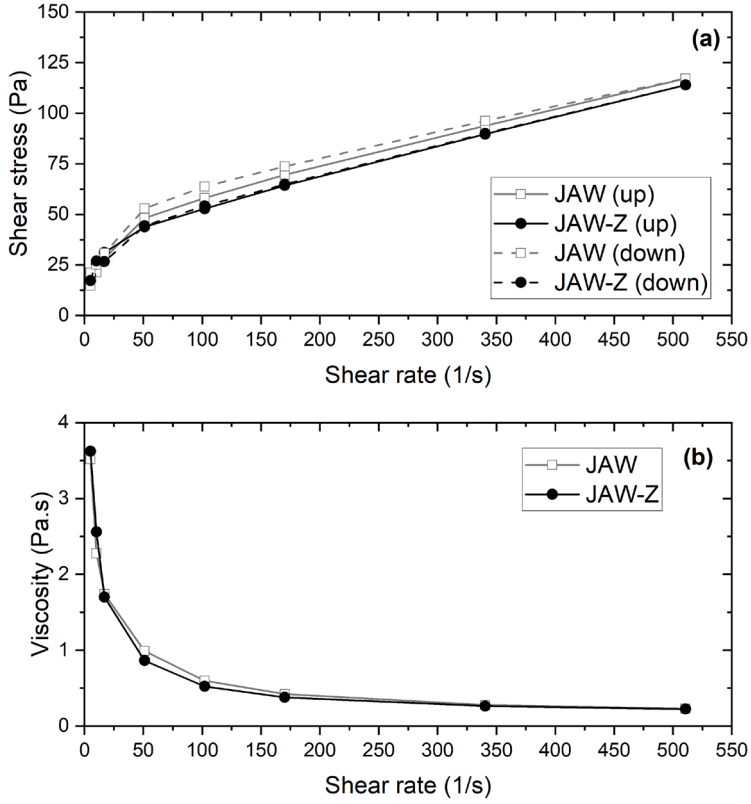

Fig. 1—(a) Shear rate-shear stress profiles and (b) viscosity curves; JAW (neat) and JAW-Z (JAW + 0.86% ZnO).

observed by Salehi et al. (2018) and Paiva et al. (2018), suggesting that geopolymers are temperature-sensitive materials, independently of their neat designs. At 20°C BHCT, both recipes had the longest pumpability duration up to 6 hours, while at 50°C BHCT, they had the shortest pumpability duration down to 45 minutes. Although the 0.86% ZnO was not effective to further elongate the thickening time compared with the neat JAW, at any of the temperatures, it mildly accelerated the setting to reach an early and sustainable strength

Mix Design	10-Second API Gel-Strength (Pa)	10-Minute API Gel-Strength (Pa)	Estimated Yield Stress (Pa)	Flow Index	Rheological Behavior
JAW	20.05	23.51	13.7	0.37	Shear thinning
JAW-Z	18.48	19.05	15.4	0.37	Shear thinning

Table 6—Rheological properties data in ambient conditions.

Mix Design	Slurry Density	Slurry pH	Slurry Zeta Potential (mV)	Initial Consistency (Bc)
JAW	1.87	13.72 (±0.01)	25.0 (±0.16)	26.4
JAW-Z	1.89	13.84 (±0.01)	25.4 (±0.29)	27.2

Table 7—Slurry properties in ambient conditions.

Mix Design	FLT Volume (mL)	FLT Blowout Time (minutes)	Spurt Loss Volume (mL)	Pore Solution pH
JAW	27 (±0.5)	6	120.75	14.0 (±0.1)
JAW-Z	25 (±0.5)	6	111.80	14.0 (±0.1)

Table 8—FLT and pore solution results.

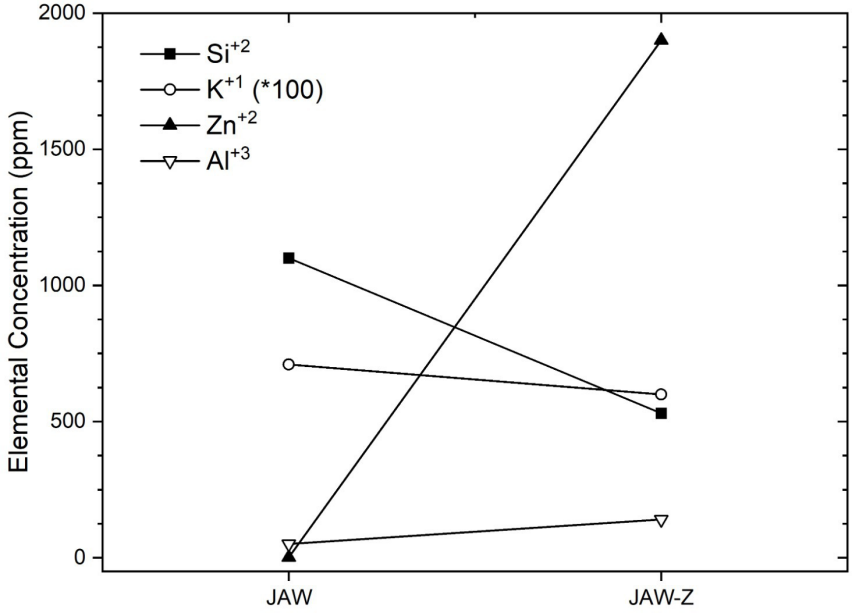

Fig. 2—Dissolution of JAW pastes using inductively coupled plasma spectrometry analysis for thier pore solutions(Omran et al. 2023b); JAW (neat) and JAW-Z (JAW + 0.86% ZnO).

development. In accordance with the DSC profiles, the dissolution of geopolymer precursors is significantly accelerated at higher temperatures. This leads to an increase in the solubility of aluminosilicates and the availability of silica ions, thereby speeding up the geopolymerization reaction and reducing the setting time (Chen et al. 2012; Pilehvar et al. 2020).

Kinetics of Pastes. **Fig. 4** and **Table 10** provide the DSC profiles and data for the two mixes and the ones from Omran et al. (2023b) at 25 and 50°C. The initial equilibration period was discarded for the given DSC curves.

Both mixes are observed to yield a single heat release peak. Chithiraputhiran and Neithalath (2013) observed a comparable single heat peak from 50 to 50 and 70 to 30 low calcium fly ash-slag geopolymers for the first 72 hours. Pilehvar et al. (2020) observed a shoulder-like shape overlapping with the single peak for a low calcium fly ash-slag geopolymer system. It would be reasonable to assume that the single peak can be identified as an indication that both the dissolution and formation of geopolymers may occur simultaneously, right after the initial mixing (Pilehvar et al. 2020; Siyal et al. 2016).

The main difference observed between the two DSC profiles in **Fig. 4** is regarding the heat release rate magnitudes and time by which they occur: The total heat released at 50°C is 5–10 times larger than the corresponding at 25°C during the first 3 hours for both mixes. This suggests a speedup rate of the dissolution and condensation processes. These observations indicate that overall geopolymerization reaction is thermally accelerated, by releasing more heat at early times and cumulative energy over time than what is observed at room temperature, as summarized in **Table 9** and similarly reported by the literature (Cai et al. 2020; Chithiraputhiran and Neithalath 2013; Ma et al. 2018; Najafi Kani et al. 2017; Omran et al. 2023b; Pilehvar et al. 2020).

At 25°C, JAW-Z paste oxide reacts earlier and has a slightly broader heat release peak than the one observed for the neat JAW at the same temperature in **Fig. 4**. The total heat release is also observed to be higher for JAW-Z. At 50°C, the first dissolution step is observed to happen very rapidly, and therefore, JAW-Z paste was able to release more heat than the neat one at the same temperature. The DSC results are also in-line with the early age sonic strength development. Omran et al. (2023b) investigated the effect of 0.5 and 0.86% ZnO in the same JAW system. They found that the higher the amount of added zinc, the higher the increase in the heat release magnitude, as well as the total amount of accumulated energy.

Early Age Sonic Strength. **Fig. 5** presents the early age sonic compressive strength performance obtained by using an ultrasonic cement analyzer (UCA). Both neat JAW and JAW-Z were measured during the first 8 hours at 70°C BHST, which is equivalent to that at 50°C BHCT. **Table 11** illustrates the results from the early age UCA.

Both recipes were observed to have comparable timing for developing strength during the initial 45 minutes, which is matching their consistency profiles and pumpability at 50°C BHCT as explained previously (see **Fig. 3**). This observation agrees with the DSC observations at 50°C BHCT, where the addition of zinc oxide is observed to have a clear effect on accelerating the early age strength development for the JAW-Z contrary to that of the neat JAW.

JAW-Z was measured to have a sonic compressive strength development of up to 8.5 MPa during the first hour of heat curing, three times higher than that of neat JAW at the same time. Furthermore, JAW-Z was observed to have a shorter hardening time to reach 3.45 MPa (500 psi) and a higher sonic strength value of up to 15.7 MPa within the first 5 hours of curing than JAW. This addition of zinc oxide also tripled the sonic compressive strength of the neat mix.

Aging Properties and Characterizations. ***Hydraulic Sealability Test.*** **Fig. 6** represents the hydraulic bond strength (HBS) profiles and breakthroughs for the injected N_2 gas over the two given JAW mix designs with the steel casing after 7 days of curing. It is important to study HBS to understand the ability of the systems to withstand pressure occurring at the cement-casing steel interface without producing a microannulus, which would compromise their integrity capacities.

The conducted HBS test acknowledges the pressure required for fluid to breakthrough the cement-steel casing interface, which was observed to happen after applying 1.5-2.0 MPa (i.e., 15–20 bars) for both mix designs. The observed results present a positive indication when being compared with the performance of OPC for well-cementing applications (Gomado et al. 2023; Salehi et al. 2018).

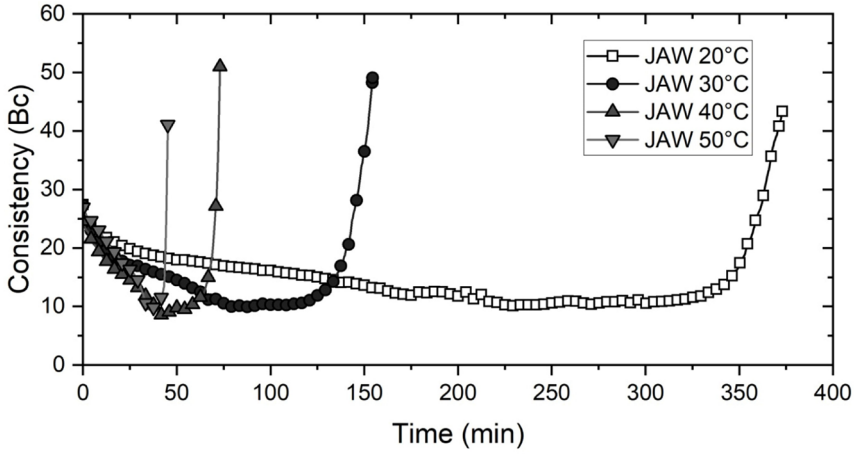

a) JAW

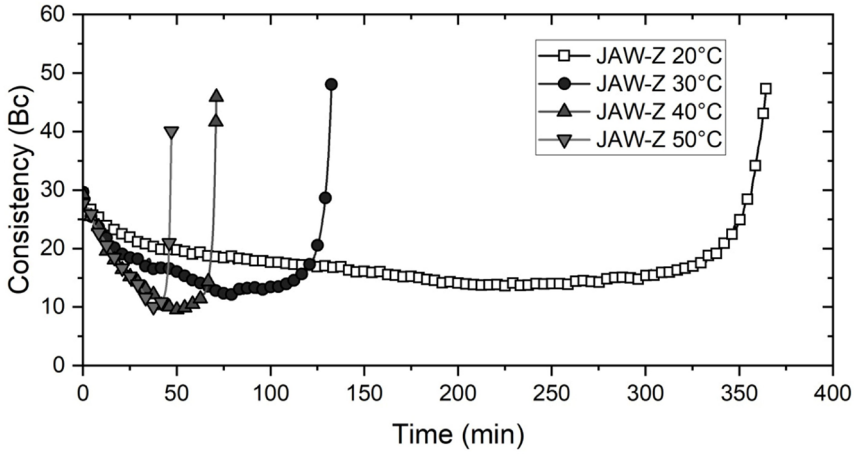

b) JAW-Z

Fig. 3—Effect of temperature on consistency of the slurries (a) JAW and (b) JAW-Z; JAW (neat) and JAW-Z (JAW + 0.86% ZnO).

Recipe/Circulating Temperature (°C BHCT)	20°C BHCT	30°C BHCT	40°C BHCT	50°C BHCT
JAW pumpability (minutes)	369.5	151.8	72.4	45.2
JAW-Z pumpability (minutes)	361.3	142.7	71.0	44.9

Table 9—Pumpability of JAW and JAW-Z at 40 Bc.

On the other hand, the aged, cured JAW sample for 1 month could not withstand 0.5 MPa with an observable de-bonding from the casing. **Fig. 7** presents the observed de-bonding and breakthrough of the injected gas at 0.5 MPa from all sides of the geopolymer-casing interface. This de-bonding could be due to shrinkage of the slurries. Salehi et al. (2018) examined the shrinkage of geopolymers. They observed that geopolymers continuously shrink with time, especially at higher curing temperatures, up to 2.5% volumetric shrinkage after 14 days. However, some geopolymers shrink with lower rates compared with OPC-based cement (Salehi et al. 2018). The observed de-bonding or shrinkage could be due to the reactants' consumption during JAW geopolymerization process as shown in **Fig. 7**. In-line with the following FTIR and XRD results and characterizations, it could happen due to having the volume of the geopolymerization products less than the given reactants, or so-called chemical shrinkage phenomenon, over time. The chemical shrinkage in geopolymers can be the result of the formation of K(Na)-A-S-H gels and/or water as byproduct of the geopolymerization reaction.

Hence, an expansive agent additive might be required to further improve the long-term HBS of the given JAW mixes. Additionally, cement slurry linear expansion and/or contraction test is required to quantify the shrinkage of the systems.

Uniaxial and Ultrasonic Strength Development. **Fig. 8** shows the uniaxial compressive strength of the geopolymer mixes (JAW and JAW-Z) after 1 day up to 56 days cured in atmospheric pressure, at 25 and 70°C BHST, respectively. **Fig. 9** and **Table 12** present the extended sonic strength development profiles and data for JAW vs. JAW-Z, at 70°C BHST and pressurized to 13.8 MPa.

At a fixed curing temperature, either 25 or 70°C BHST, it is observed that the longer the specimen is allowed to cure, the higher the uniaxial compressive strength is obtained for both recipes, in-line with (Chithiraputhiran and Neithalath 2013). Hence, one may also conclude that with a higher curing temperature, higher geopolymer strength development should be expected (Chithiraputhiran and Neithalath 2013; Salehi et al. 2018). Furthermore, the addition of ZnO gave an effective and clear early age strength booster effect on JAW-Z, in-line with the discussed DSC results (see **Fig. 4**). The addition of this strength booster has doubled and tripled the UCS after

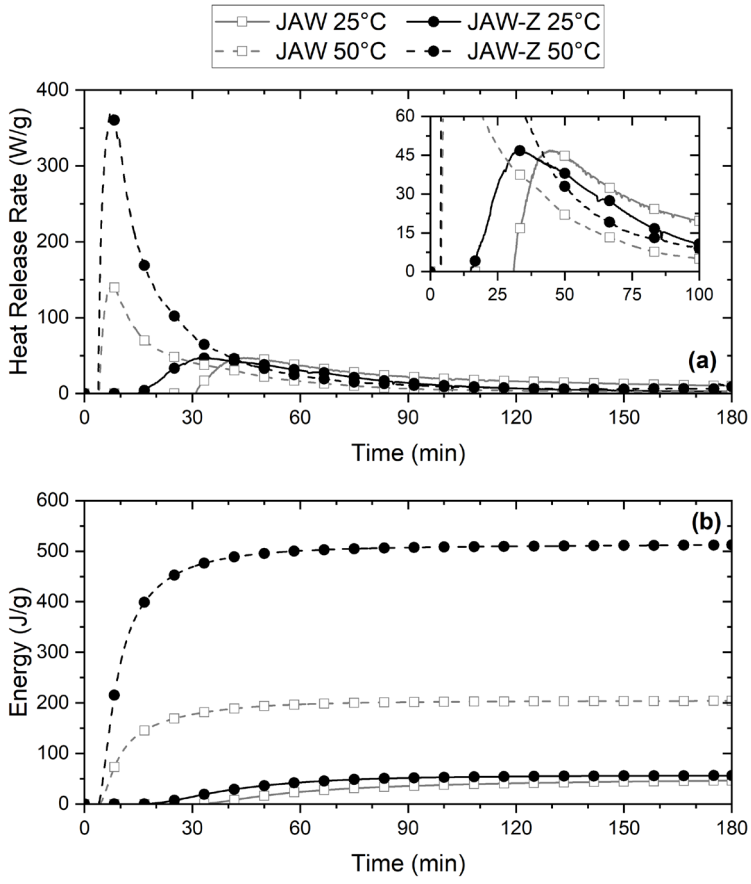

Fig. 4—DSC data: (a) heat rate and (b) energy release; JAW (neat) and JAW-Z (JAW + 0.86% ZnO).

	Time at Maximum Heat Release Rate (minutes)		Maximum Heat Release Rate (mW/g)		Total Energy Release (J/g)	
Material	25°C BHCT	50°C BHCT	25°C BHCT	50°C BHCT	25°C BHCT	50°C BHCT
JAW	47	8	47	143	46	204
JAW-Z	33	7	47	372	56	512

Table 10—Kinetics data for JAW and JAW-Z.

1 day of curing in ambient and elevated temperatures, respectively. This observation agrees with the numbers obtained from the UCA data as seen previously in **Fig. 5**. In addition, others have stated the positive effects of utilizing zinc compounds for AAM that can improve the cementing properties, including compressive strength development (Hajimohammadi et al. 2011; Luukkonen et al. 2018; Van et al. 2012). One may conclude that the addition of ZnO is very crucial to develop acceptable and durable mechanical properties for well cementing, especially for low-to-medium temperature applications.

From the extended UCA profiles seen in **Fig. 8**, two sonic strength development zones can be identified for both recipes. The first development curve is observed to happen around the initial mixing and early age curing which lasted for 2 weeks for JAW and 3 weeks for JAW-Z. Continuing, the second development curve was observed to be a long-term asymptotically like increasing function curve for both mixes. The presence of the second strength development curve could be an indication of an additional internal structural reorganization and participation of the remaining unreacted precursor particles, which is aligned with the hydraulic sealability data, although in different time scales. This could be an interesting observation, especially considering quartz present in granite. Further investigation on the consecutive reaction could provide a better understanding of the product, resulting in more favorable long-term mature geopolymerization products, which yield favorable mechanical properties.

After 28 days of heat curing at 70°C BHST, the UCS of JAW subdued the UCS for JAW-Z. This observation matches with the values obtained from the UCA, where JAW started to positively overcome JAW-Z. The sonic strength of the neat JAW after 28 and 56 days are 28 and 42 MPa, respectively, while for JAW-Z are 16 and 31 MPa, respectively. These extended UCA results are very comparable with the extended UCS results. A comparable trend was observed by Van et al. (2012) in calcium-rich AAM using ZnO as a chemical admixture.

Fourier-Transform Infrared Spectroscopy. Figs. 10 and 11 and **Tables 13 through 16** present the FTIR spectra and wave hollow data of the two recipes. The mix designs were studied after 7, 28, and 56 days of curing at 25 and 70°C BHST, respectively. The band

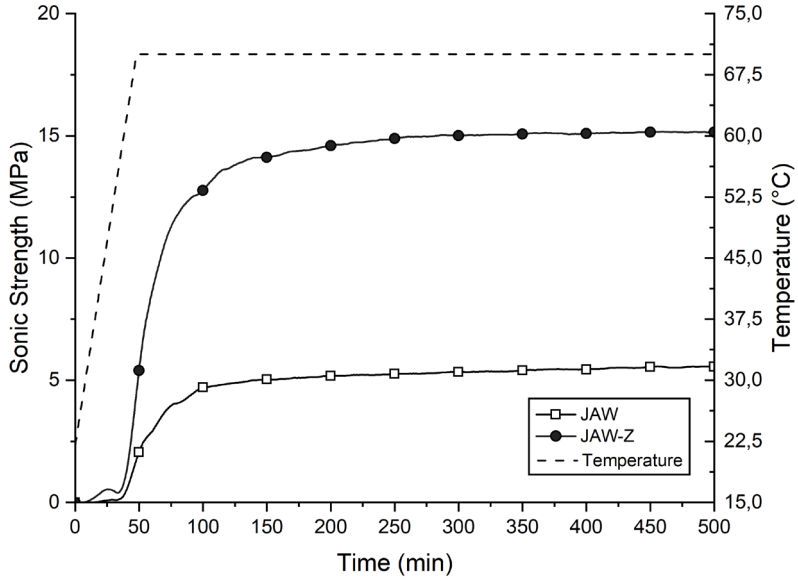

Fig. 5—Ultrasonic cement analyzer early age profile at 70°C bottom hole static temperature (BHST) and 13.8 MPa; JAW (neat) and JAW-Z (JAW + 0.86% ZnO).

Mix Design	Setting Time to 100 psi (minutes)	Hardening Time to 500 psi (minutes)	Sonic Strength (MPa) for 1 hour	Sonic Strength (MPa) for 5 hours
JAW	43	66	2.8	5.9
JAW-Z	38	46	8.5	15.7

Table 11—UCA early age data (Omran et al. 2023b).

in the range of 1400–700 cm^{-1} is assigned to the T-O-T (T is a tetrahedral Si or Al) bond asymmetric stretching vibrations. The T-O-T band position can indicate the dissolution of the aluminosilicate source, gelatinous product formations, and degree of crosslinking within the geopolymerization network. Absorption O-C-O band between 1500 and 1400 cm^{-1} is assigned to the presence of calcium and CO_3^{-2} groups. The intensity of the broad hump in ranges of 3600–3000 cm^{-1} and 1700–1600 cm^{-1} is associated with the presence of H-OH group stretching vibrations (Ma et al. 2018, 2019).

The results obtained from running FTIR show broad stretching vibrations and shifting in the bands' positions for JAW and JAW-Z as a function of curing time and curing temperature. At 25°C, JAW and JAW-Z have the T-O-T stretching vibrations in ranges between 1400 and 700 (cm^{-1}), which are centered around 962–966 (cm^{-1}) after 7 days of curing for then to be centered around 975 (cm^{-1}) after 56 days. This shift in the wavelength of T-O-T bands for JAW and JAW-Z can be correlated to the dissolution of aluminosilicate precursor (Hajimohammadi et al. 2011), and the formation of CASH, NASH, or both gels with a higher crosslinking degree. Hence, the addition of

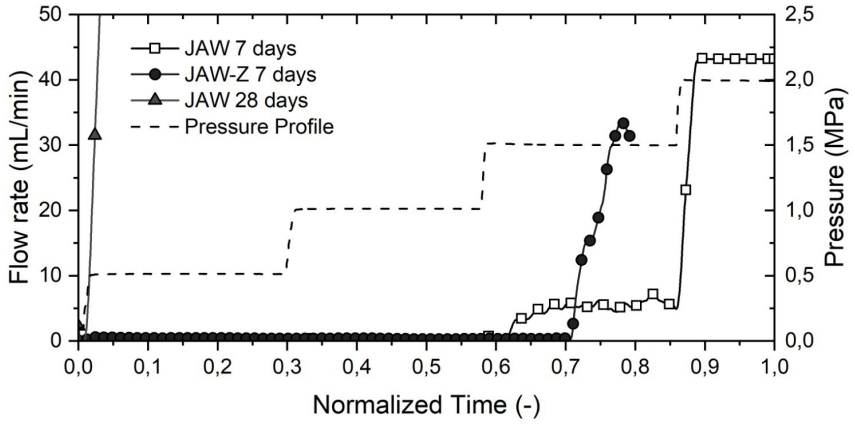

Fig. 6—Hydraulic sealability for JAW and JAW-Z mixes. The first gray arrow is the partial initial breakthrough at 1.5 MPa for the neat JAW; the second gray arrow is the complete breakthrough between 1.5-2.0 MPa for the neat JAW. The black arrow is the complete breakthrough at 1.5 MPa for JAW-Z.

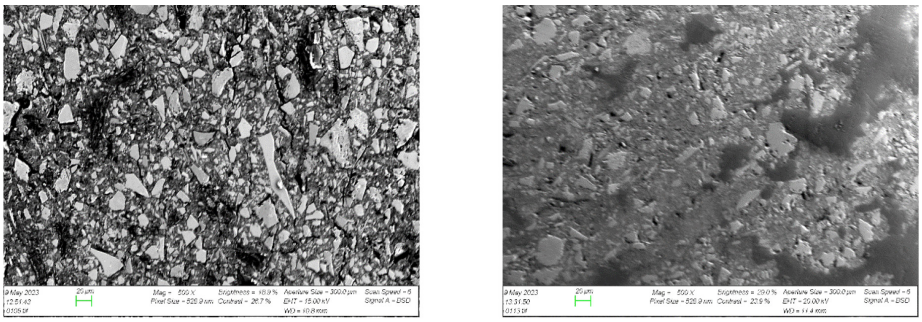

a) mainly geopolymer reactants b) mainly geopolymer products

c) gas breakthrough during the hydraulic bond strength test

Fig. 7—(a) SEM image of early age JAW mix, (b) SEM image of aged JAW mix, and (c) top view of the sealability cell after debonding of the aged JAW.

admixtures could be low enough not to cause a significant influence on FTIR peaks around 1100 – 1000 cm^{-1} (Hajimohammadi et al. 2011). Interestingly, the size of T-O-T bands for both mixes with aging was getting smaller which might be correlated to the further dissolution and participation of granite. This could define and be in-line with the presence of the second sonic strength development zone in **Fig. 8**.

The C-O-C vibration is hard to detect clearly due to the low calcium content in the mix designs, which agrees with previous studies (Omran et al. 2023b). The H-OH stretching at 3600–3000 cm^{-1} and 1700–1600 cm^{-1} is comparable for both JAW and JAW-Z. Hence, the resonance intensity differences are a function of the composition and concentration of the reaction products. This trend can be also observed at 70°C BHST curing, but with a higher shifting of the wavelengths for T-O-T and H-OH bands. These shifts indicate a higher degree of geopolymerization happening at elevated curing temperatures in agreement with Shah et al. (2020). Therefore, the longer the

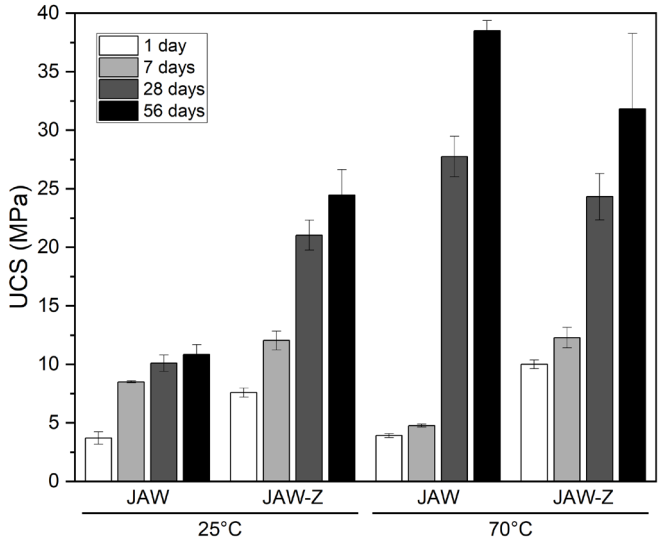

Fig. 8—UCS data at 25 and 70°C BHST.

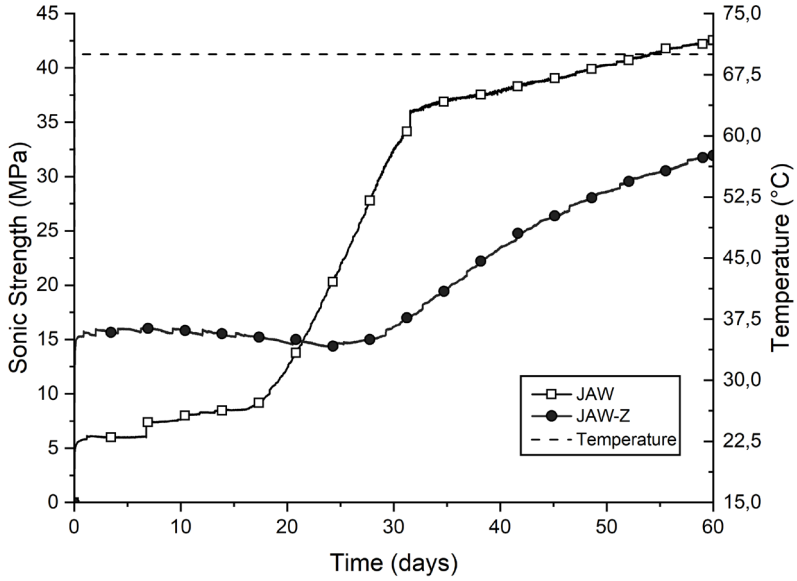

Fig. 9—UCA profiles for JAW and JAW-Z; JAW (neat) and JAW-Z (JAW + 0.86% ZnO).

Sonic Strength (Day)	1D	7D	14D	28D	56D	60D
JAW (MPa)	5.8	7.4	8.5	28.4	41.8	42.4
JAW-Z (MPa)	15.8	16.0	15.7	15.5	30.7	31.9

Table 12—Extended UCA sonic strength development data up to 2 months.

specimen is allowed to cure while undergoing higher curing temperature, the higher the shifts in T-O-T, Si-O, and H-OH bonds are to be expected. Afterward, the higher the formation of silicate hydration products in higher amounts could be produced and detected.

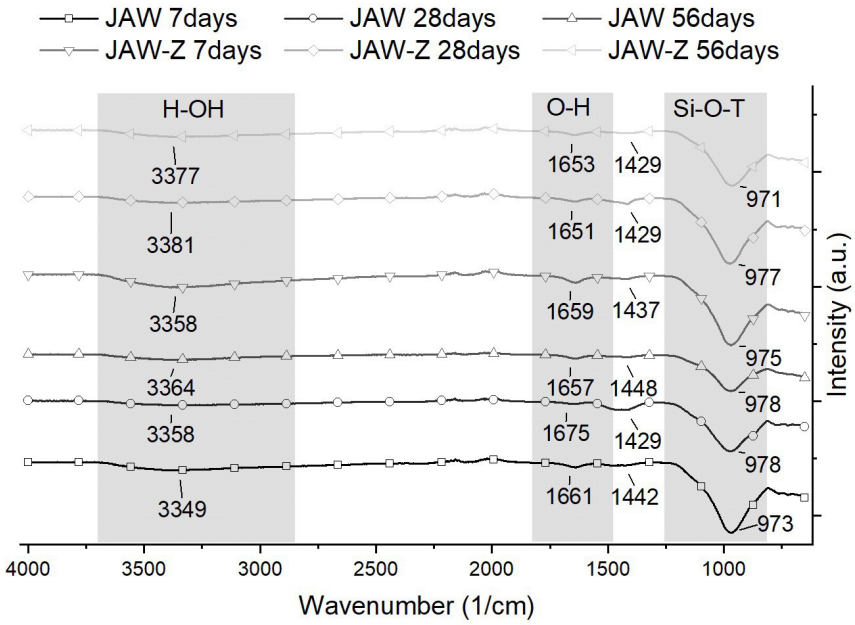

Fig. 10—FTIR for JAW and JAW-Z at 25°C BHST.

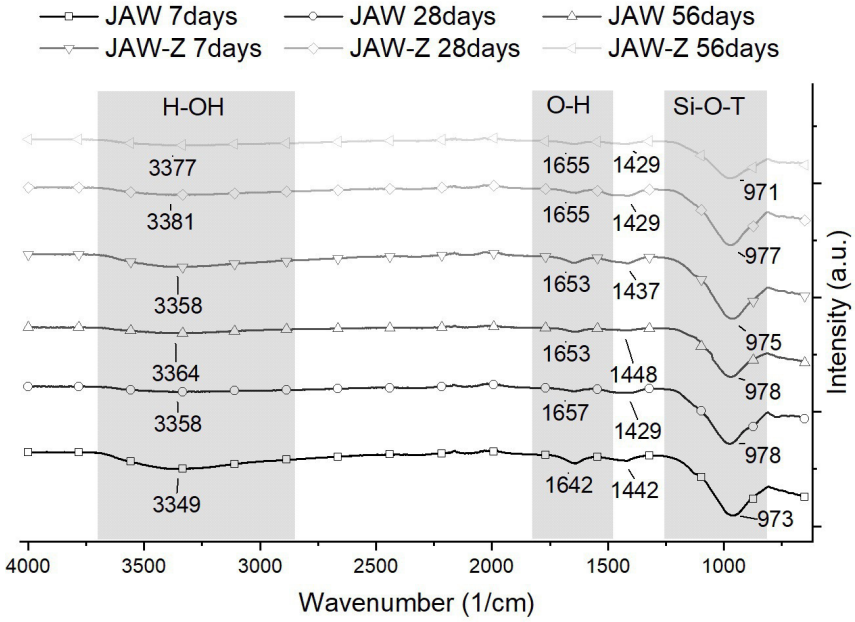

Fig. 11—FTIR for JAW vs. JAW-Z at 70°C BHST.

Mix Design (25°C)	Curing Duration	T-O-T (cm^{-1}) (1400–700)	H-OH (cm^{-1}) (1700–1600)	H-OH (cm^{-1}) (3600–3000)
JAW	7D	973	1661	3349
JAW	28D	978	1675	3358
JAW	56D	978	1657	3364

Table 13—The wave hollows occurred for JAW at 25°C BHST.

Mix Design (25°C)	Curing Duration	T-O-T (cm^{-1}) (1400–700)	H-OH (cm^{-1}) (1700–1600)	H-OH (cm^{-1}) (3600–3000)
JAW-Z	7D	975	1659	3358
JAW-Z	28D	977	1651	3381
JAW-Z	56D	971	1653	3377

Table 14—The wave hollows occurred for JAW-Z at 25°C BHST.

Mix Design (70°C)	Curing Duration	T-O-T (cm^{-1}) (1400–700)	H-OH (cm^{-1}) (1700–1600)	H-OH (cm^{-1}) (3600–3000)
JAW	7D	973	1642	3349
JAW	28D	978	1657	3358
JAW	56D	978	1653	3364

Table 15—The wave hollows occurred for JAW at 70°C BHST.

Mix Design (70°C)	Curing Duration	T-O-T (cm^{-1}) (1400–700)	H-OH (cm^{-1}) (1700–1600)	H-OH (cm^{-1}) (3600–3000)
JAW-Z	7D	975	1653	3358
JAW-Z	28D	977	1655	3381
JAW-Z	56D	971	1655	3377

Table 16—The wave hollows occurred for JAW-Z at 70°C BHST.

Minerals	(No.)	Granite (%wt/wt)
Quartz	PDF 00-008-7651	35.693
Albite	PDF 00-009-0466	21.625
Microcline 1	CIF 9004191	16.059
Microcline 2	PDF 00-019-0932	11.918
Oligoclase	CIF 9011423	10.654
Biotite	PDF 04-013-2135	2.382
Chlorite	COD 9010163	1.669

Table 17—Granite mineralogy obtained from Rietveld quantification (Omran et al. 2023b).

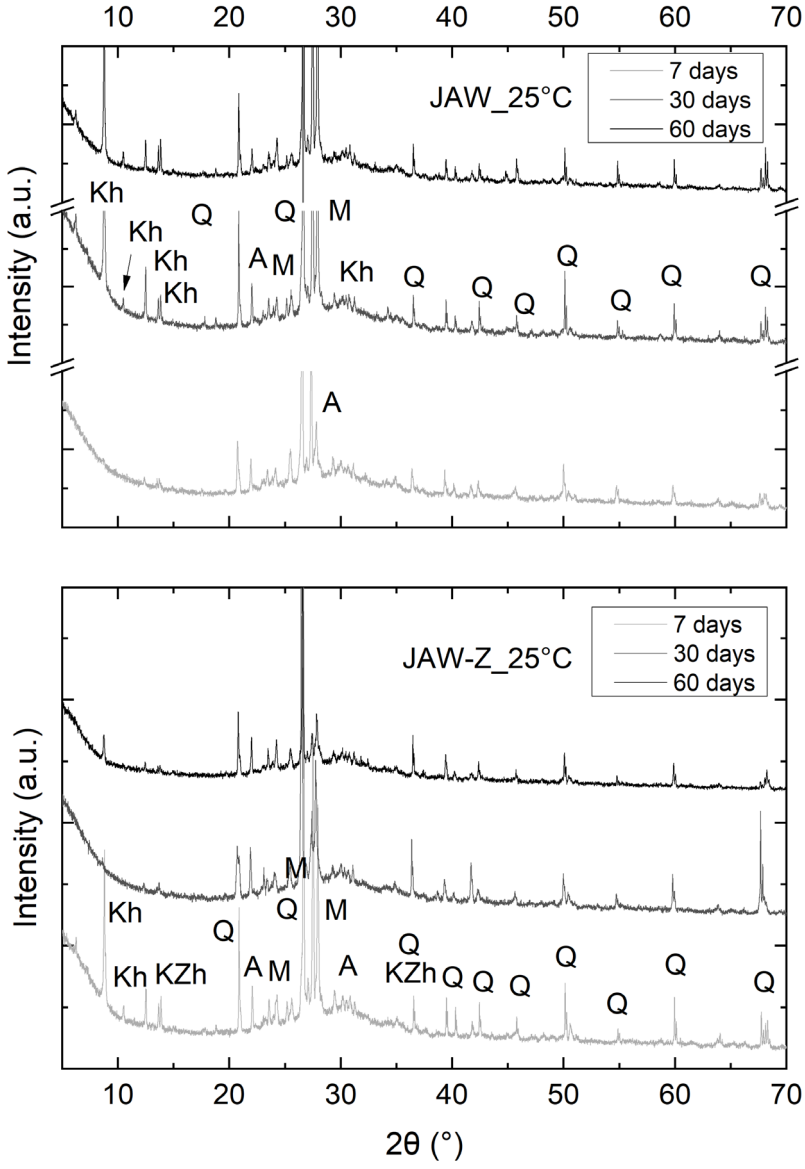

Fig. 12—XRD patterns of JAW (neat) and JAW-Z (JAW + 0.86% ZnO), both cured at 25°C BHST. Q, quartz; M, microcline; A, albite; Kh, K-A-S-H or C-K-A-S-H; KZh, K-Z-A-S-H.

X-ray Diffraction. Omran et al. (2023a, 2023b) characterized the precursors granite, GGBFS, and MS using XRD and Rietveld refinement. The results exhibited granite to be a highly crystalline precursor, rich in quartz, feldspar (microcline and albite), and oligoclase, with biotite and chlorite as minor phases, with a crystalline content of around 80% (see **Table 17**). While GGBFS and MS have highly amorphous content.

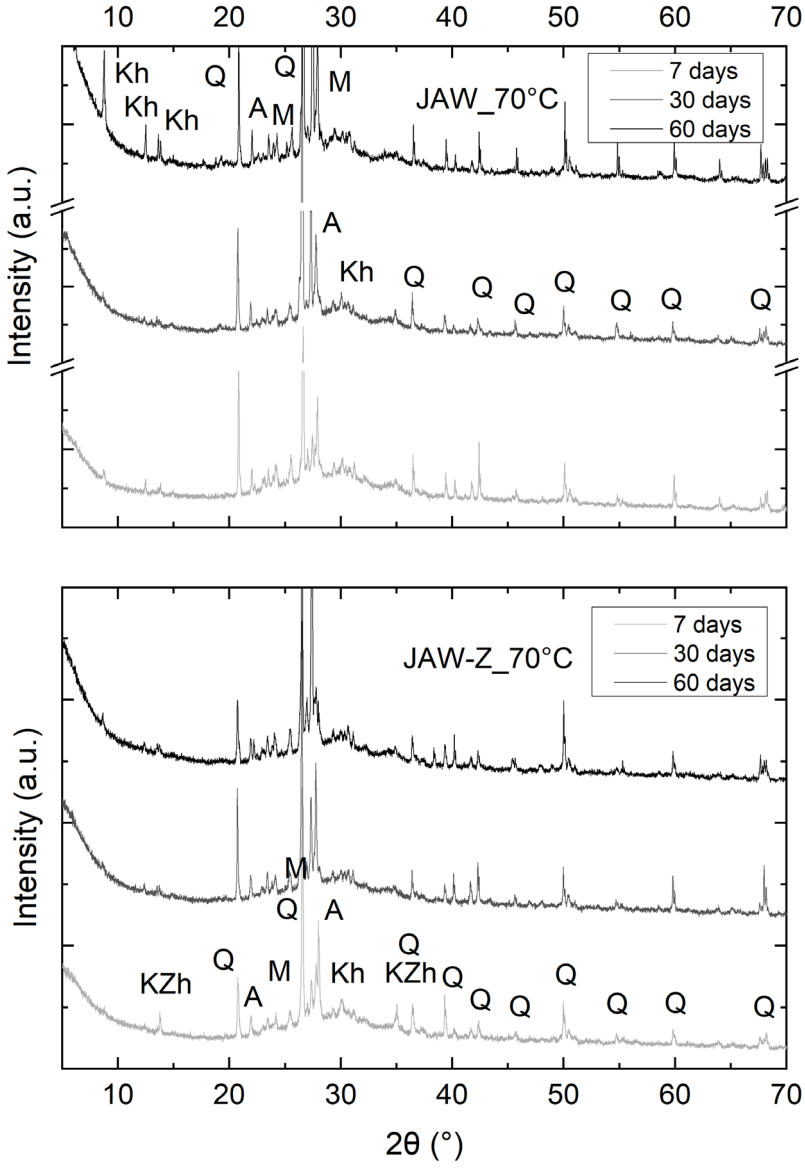

Fig. 13—XRD patterns of JAW (neat) and JAW-Z (JAW + 0.86% ZnO), both cured at 70 °C BHST. Q, quartz; M, microcline; A, albite; Kh, K-A-S-H or C-K-A-S-H; KZh, K-Z-A-S-H.

The XRD peaks and patterns of JAW and JAW-Z after 7D, 28D, and 56D under 25 and 70°C BHST are illustrated in **Figs. 12 and 13**, respectively.

XRD patterns of JAW and JAW-Z have also been investigated as functions of curing time and curing temperature. The XRD peak intensities became higher and more crystalline by increasing both the curing period and curing temperature. These observed results match (Hajimohammadi et al. 2011; Pilehvar et al. 2020; Samantasinghar and Singh 2019) considering low calcium content AAM due to the overlaying of natural and synthesized crystals between angles 20–30° 2θ.

On the other hand, this trend could not be observed for the JAW-Z mix at 25°C, where XRD reveals a much higher amorphous content. The presence of the amorphous phases can be due to the unreacted amorphous precursor phases. Both mixes may potentially contain amorphous geopolymers and hydrated phases such as C-A-S-H and C-(K, Na)-A-S-H, or a mix of both combined. Therefore, it would be fair to assume that JAW-Z could also contain an additional K-Zn-A-S-H phase as seen in **Figs. 10 and 11**. These XRD observations are in-line with previous studies (Omran et al. 2023b; Omran and Khalifeh 2023).

Morphology—Scanning Electron Microscopy. Granite has irregularly crystalline-shaped particles mainly of quartz and feldspars. In addition, GGBFS and MS have a higher specific surface area and lower particle-size distribution, when compared with granite (Omran et al. 2023a). **Figs. 14 and 15** include SEM micrographs of the two mixes cured at 25 and 70°C, respectively, taken after 7D, 28D, and 56D of curing.

The SEM images reveal that curing time and temperature have impact on the formation of more dense structures. Both mixes are observed to have a higher degree of incomplete geopolymerization reactions after 7D with fewer formation of gels. Unlike that of the 7 days of curing micrographs, the 28 and 56 days of curing indicate very low to the negligible presence of any remains of unreacted particles of granite and/or GGBFS. In addition, the longer the curing duration, the lower the matrix porosity, and the denser and the harder

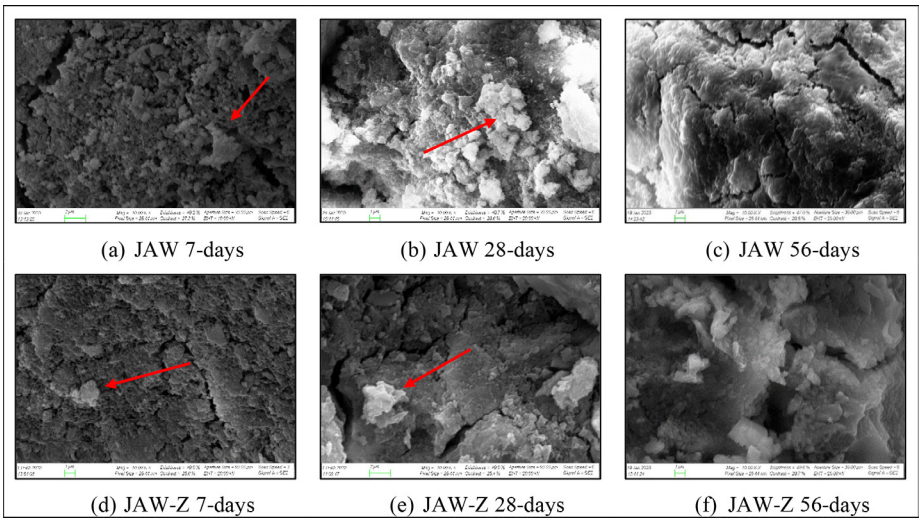

Fig. 14—SEM 25°C BHST, magnification of 10K.X. Results of curing time up to 2 months. The red arrow points toward unreacted particles; JAW (neat) and JAW-Z (JAW + 0.86% ZnO).

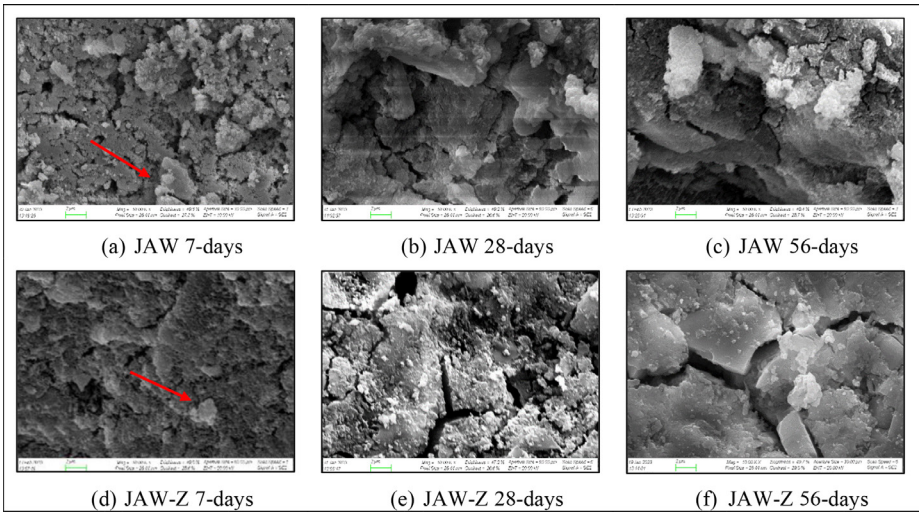

Fig. 15—SEM 70°C BHST, magnification of 10 K.X. Results of curing time up to 2 months. The red arrow points toward unreacted particles; JAW (neat) and JAW-Z (JAW + 0.86% ZnO).

the matrix gets for the two mixes. The dense matrices for JAW and JAW-Z match the results obtained from FTIR and strength development evolutions over curing time.

The variation in curing temperature is also observed to have a clear effect on the SEM micrographs for both mixes. The samples cured at 25°C show larger amounts of unreacted particles and smaller amounts of geopolymer products. Contrary, the samples cured at 70°C are observed to have fewer remaining unreacted particles and larger amounts of geopolymer products being formed. Having the samples cured at elevated temperatures is observed to accelerate the geopolymerization reaction, which then helps the geopolymerization network in forming more complex 3D structures and denser geopolymer matrixes. This trend is in-line with the literature (Pilehvar et al. 2020; Salehi et al. 2018). Furthermore, the previously mentioned SEM observations also match the results and trends obtained from FTIR and strength development evolution at prolonged curing and higher curing temperature.

Conclusion

Chemical properties and mechanical performance of aged granite-based JAW geopolymer were studied for well-cementing applications under a wide range of curing temperatures. High curing temperature favors the geopolymerization reaction, strongly impacts pumpability of the slurries, leaves fewer remaining unreacted precursor particles, improves strength development rate, and results in formation of denser structures and higher crystalline products. The use of ZnO as a strength enhancer was crucial for achieving acceptable mechanical properties in low-temperature well-cementing applications, even though it may lead to a slight reduction in compressive strength compared with the neat mix design at a later stage. However, the hydraulic sealability of the system is negatively impacted with aging JAW mixes due to de-bonding at the geopolymer-casing interface. An expansive agent might be required to further improve the long-term HBS of JAW to avoid any possible chemical shrinkage with aging.

Acknowledgments

The authors gratefully acknowledge TotalEnergies, AkerBP, ConocoPhillips, and the Research Council of Norway for financially supporting the SafeRock KPN Project (RCN 319014- New Cementitious Material for Oil Well Cementing Applications - SafeRock) at the University of Stavanger, Norway. In addition, the authors would like to acknowledge Mr. Sondre Hjelm and Mr. Foster Gomado for their laboratory contribution.

References

Adam, A. A. and Horianto, X.. 2014. The Effect of Temperature and Duration of Curing on the Strength of Fly Ash Based Geopolymer Mortar. *Procedia Eng* **95**: 410–414. https://doi.org/10.1016/j.proeng.2014.12.199.

Anseau, M. R., Leung, J. P., Sahai, N. et al. 2005. Interactions of Silicate Ions with Zinc(II) and Aluminum(III) in Alkaline Aqueous Solution. *Inorg Chem* **44** (22): 8023–8032. https://doi.org/10.1021/ic050594c.

API RP 10B-2, *Recommended Practice for Testing Well Cements*. 2019. Washington, DC: American Petroleum Institute.

Cai, J., Li, X., Tan, J. et al. 2020. Thermal and Compressive Behaviors of Fly Ash and Metakaolin-Based Geopolymer. *J Build Eng* **30**: 101307. https://doi.org/10.1016/j.jobe.2020.101307.

Chamssine, F. 2023. *Instituting Retarders for Geopolymers Developed for Downhole Applications*. PhD thesis, University of Stavanger, Stavanger, Norway.

Chen, A., Xu, D., Chen, X. et al. 2012. Measurements of Zinc Oxide Solubility in Sodium Hydroxide Solution from 25 to 100 °C. *Trans Nonferrous Met Soc* **22** (6): 1513–1516. https://doi.org/10.1016/S1003-6326(11)61349-6.

Chithiraputhiran, S. and Neithalath, N. 2013. Isothermal Reaction Kinetics and Temperature Dependence of Alkali Activation of Slag, Fly Ash and Their Blends. *Constr Build Mater* **45**: 233–242. https://doi.org/10.1016/j.conbuildmat.2013.03.061.

Gilfillan, D. and Marland, G. 2021. CDIAC-FF: Global and National CO_2 Emissions from Fossil Fuel Combustion and Cement Manufacture: 1751–2017. *Earth Syst Sci Data* **13** (4): 1667–1680. https://doi.org/10.5194/essd-13-1667-2021.

Gomado, F. D., Khalifeh, M., and Aasen, J. A. 2023. Expandable Geopolymers for Improved Zonal Isolation and Plugging. Paper presented at the SPE/IADC International Drilling Conference and Exhibition, SPE, Stavanger, Norway, 9 March. https://doi.org/10.2118/212493-MS.

Hajimohammadi, A. and van Deventer, J. S. J. 2017. Characterisation of One-Part Geopolymer Binders Made from Fly Ash. *Waste Biomass Valor* **8** (1): 225–233. https://doi.org/10.1007/s12649-016-9582-5.

Hajimohammadi, A., Provis, J. L., and van Deventer, J. S. J. 2008. One-Part Geopolymer Mixes from Geothermal Silica and Sodium Aluminate. *Ind Eng Chem Res* **47** (23): 9396–9405. https://doi.org/10.1021/ie8006825.

Hajimohammadi, A., Provis, J. L., and van Deventer, J. S. J. 2011. Time-Resolved and Spatially-Resolved Infrared Spectroscopic Observation of Seeded Nucleation Controlling Geopolymer Gel Formation. *J Colloid Interface Sci* **357** (2): 384–392. https://doi.org/10.1016/j.jcis.2011.02.045.

Hjelm, S. 2022. *Revealing the Effect of Superplasticizers on Viscosity and Yield Stress of Geopolymers*. Bachelor thesis, University of Stavanger, Stavanger, Norway.

Ke, X., Bernal, S. A., Ye, N. et al. 2015. One-Part Geopolymers Based on Thermally Treated Red Mud/NaOH Blends. *J Am Ceram Soc* **98** (1): 5–11. https://doi.org/10.1111/jace.13231.

Khalifeh, M. 2016. *Materials for Optimized P&A Performance: Potential Utilization of Geopolymers*. PhD Thesis, University of Stavanger, Stavanger, Norway.

Khalifeh, M., Saasen, A., Hodne, H. et al. 2018. Geopolymers as an Alternative for Oil Well Cementing Applications: A Review of Advantages and Concerns. *J Energy Resour Technol* **140** (9): 092801. https://doi.org/10.1115/1.4040192.

Khalifeh, M., Saasen, A., Hodne, H. et al. 2019. Laboratory Evaluation of Rock-Based Geopolymers for Zonal Isolation and Permanent P&A Applications. *J Pet Sci Eng* **175**: 352–362. https://doi.org/10.1016/j.petrol.2018.12.065.

Kong, D. L. Y. and Sanjayan, J. G. 2010. Effect of Elevated Temperatures on Geopolymer Paste, Mortar and Concrete. *Cem Concr Res* **40** (2): 334–339. https://doi.org/10.1016/j.cemconres.2009.10.017.

Li, X., Wang, Z., and Jiao, Z. 2013. Influence of Curing on the Strength Development of Calcium-Containing Geopolymer Mortar. *Materials (Basel)* **6** (11): 5069–5076. https://doi.org/10.3390/ma6115069.

Luukkonen, T., Abdollahnejad, Z., Yliniemi, J. et al. 2018. One-Part Alkali-Activated Materials: A Review. *Cem Concr Res* **103**: 21–34. https://doi.org/10.1016/j.cemconres.2017.10.001.

Ma, C., Long, G., Shi, Y. et al. 2018. Preparation of Cleaner One-Part Geopolymer by Investigating Different Types of Commercial Sodium Metasilicate in China. *J Clean Prod* **201**: 636–647. https://doi.org/10.1016/j.jclepro.2018.08.060.

Ma, C., Zhao, B., Guo, S. et al. 2019. Properties and Characterization of Green One-Part Geopolymer Activated by Composite Activators. *J Clean Prod* **220**: 188–199. https://doi.org/10.1016/j.jclepro.2019.02.159.

Mahendra, K. and Narasimhan, M. C. 2023. One Part Alkali-Activated Materials for Construction – A Review. *Materials Today: Proceedings*. https://doi.org/10.1016/j.matpr.2023.07.116.

McLellan, B. C., Williams, R. P., Lay, J. et al. 2011. Costs and Carbon Emissions for Geopolymer Pastes in Comparison to Ordinary Portland Cement. *J Clean Prod* **19** (9–10): 1080–1090. https://doi.org/10.1016/j.jclepro.2011.02.010.

Mellado, A., Catalán, C., Bouzón, N. et al. 2014. Carbon Footprint of Geopolymeric Mortar: Study of the Contribution of the Alkaline Activating Solution and Assessment of an Alternative Route. *RSC Adv* **4** (45): 23846–23852. https://doi.org/10.1039/C4RA03375B.

Mo, L., Deng, M., and Tang, M. 2010. Effects of Calcination Condition on Expansion Property of MgO-Type Expansive Agent Used in Cement-Based Materials. *Cem Concr Res* **40** (3): 437–446. https://doi.org/10.1016/j.cemconres.2009.09.025.

Najafi Kani, E., Allahverdi, A., and Provis, J. L. 2017. Calorimetric Study of Geopolymer Binders Based on Natural Pozzolan. *J Therm Anal Calorim* **127** (3): 2181–2190. https://doi.org/10.1007/s10973-016-5850-7.

Nematollahi, B., Sanjayan, J., and Shaikh, F. U. A. 2015. Synthesis of Heat and Ambient Cured One-Part Geopolymer Mixes with Different Grades of Sodium Silicate. *Ceram Int* **41** (4): 5696–5704. https://doi.org/10.1016/j.ceramint.2014.12.154.

Omran, M. 2023. *Synthesis and Development of One-Part Rock-Based Geopolymers for Well Cementing Applications*. PhD theses UiS; 717, University of Stavanger, Stavanger, Norway.

Omran, M., Hjelm, S., Khalifeh, M. et al. 2023a. Synthesis of Sustainable One-Part Geopolymers for Well Cementing Applications. *Geoenergy Sci Eng* **227**: 211822. https://doi.org/10.1016/j.geoen.2023.211822.

Omran, M. and Khalifeh, M. 2022. Development of Low Carbon Dioxide Intensive Rock-Based Geopolymers for Well Cementing Applications – One-Part Geopolymer. Paper presented at the ASME 2022 41st International Conference on Ocean, Offshore and Arctic Engineering, Hamburg, Germany, 5–10 June. https://doi.org/10.1115/OMAE2022-78535.

Omran, M. and Khalifeh, M. 2023. Development of One-Part Rock-Based Geopolymers for Downhole Cementing Applications. *J Energy Resour Technol* **145** (10): 103201. https://doi.org/10.1115/1.4062250.

Omran, M., Khalifeh, M., and Hjelm, S. 2022b. Role of Zeta Potential on Rheology of One-Part Geopolymer Slurries: Influence of Superplasticizers. Paper presented at the Annual Transactions of the Nordic Rheology Society Vol. 30, Reykjavik, Iceland.

Omran, M., Khalifeh, M., and Saasen, A. 2022a. Influence of Activators and Admixtures on Rheology of Geopolymer Slurries for Well Cementing Applications. Paper presented at the SPE Asia Pacific Oil & Gas Conference and Exhibition, Adelaide, Australia, 17–19 October. https://doi.org/10.2118/210698-MS.

Omran, M., Paiva, M., and Khalifeh, M. 2023b. Design and Early Age Performance of Sustainable One-Part Geopolymers for Well Cementing. *SPE J.* **28** (5): 2675–2692. https://doi.org/10.2118/215825-PA.

Paiva, M. D. M., Silva, E. C. C. M., Melo, D. M. A. et al. 2018. A Geopolymer Cementing System for Oil Wells Subject to Steam Injection. *J Pet Sci Eng* **169**: 748–759. https://doi.org/10.1016/j.petrol.2018.06.022.

Pilehvar, S., Sanfelix, S. G., Szczotok, A. M. et al. 2020. Effect of Temperature on Geopolymer and Portland Cement Composites Modified with Micro-Encapsulated Phase Change Materials. *Constr Build Mater* **252**: 119055. https://doi.org/10.1016/j.conbuildmat.2020.119055.

Rovnaník, P. 2010. Effect of Curing Temperature on the Development of Hard Structure of Metakaolin-Based Geopolymer. *Constr Build Mater* **24** (7): 1176–1183. https://doi.org/10.1016/j.conbuildmat.2009.12.023.

Salehi, S., Khattak, M. J., Ali, N. et al. 2018. Study and Use of Geopolymer Mixtures for Oil and Gas Well Cementing Applications. *J Energy Resour Technol* **140** (1): 1–12. https://doi.org/10.1115/1.4037713.

Samantasinghar, S. and Singh, S. P. 2019. Fresh and Hardened Properties of Fly Ash–Slag Blended Geopolymer Paste and Mortar. *Int J Concr Struct Mater* **13** (1): 47. https://doi.org/10.1186/s40069-019-0360-1.

Shah, S. F. A., Chen, B., Oderji, S. Y. et al. 2020. Improvement of Early Strength of Fly Ash-Slag Based One-Part Alkali Activated Mortar. *Constr Build Mater* **246**: 118533. https://doi.org/10.1016/j.conbuildmat.2020.118533.

Singh, N. B. and Middendorf, B. 2020. Geopolymers as an Alternative to Portland Cement: An Overview. *Constr Build Mater* **237**: 117455. https://doi.org/10.1016/j.conbuildmat.2019.117455.

Siyal, A. A., Azizli, K. A., Man, Z. et al. 2016. Effects of Parameters on the Setting Time of Fly Ash Based Geopolymers Using Taguchi Method. *Procedia Eng* **148**: 302–307. https://doi.org/10.1016/j.proeng.2016.06.624.

Sun, Z. and Vollpracht, A. 2019. One Year Geopolymerisation of Sodium Silicate Activated Fly Ash and Metakaolin Geopolymers. *Cem Concr Compos* **95**: 98–110. https://doi.org/10.1016/j.cemconcomp.2018.10.014.

Van, J. S. J., Duxson, P., Brice, D. G. et al. 2012. *Settable Composition Comprising Slag*. WO2012083384A.